SCIENTIFIC REPORTS

OPEN

Received: 08 July 2015
Accepted: 05 October 2015
Published: 30 October 2015

Facile Synthesis of Defective TiO_{2-x} Nanocrystals with High Surface Area and Tailoring Bandgap for Visible-light Photocatalysis

Muhammad Wajid Shah[1,2], Yunqing Zhu[1], Xiaoyun Fan[1], Jie Zhao[1], Yingxuan Li[1], Sumreen Asim[1,2] & Chuanyi Wang[1]

A facile hydrothermal approach has been developed to prepare defective TiO_{2-x} nanocrystals using Ti(III)-salt as a precursor and *L*-ascorbic acid as reductant and structure direction agent. The prepared TiO_{2-x} nanocrystals are composed of a highly crystallized TiO_2 core and a disordered TiO_{2-x} outer layer, possessing high surface area, controlled oxygen vacancy concentration and tunable bandgap via simply adjusting the amount of added *L*-ascorbic acid. The defective TiO_{2-x} shows high photocatalytic efficiency in methylene blue and phenol degradation as well as in hydrogen evolution under visible light, underlining the significance of the present strategy for structural and bandgap manipulation in TiO_2-based photocatalysis.

TiO_2 is one of extensively studied photocatalytic materials due to its excellent physicochemical properties as well as its earth abundance, nontoxicity and stability[1–4]. However, the large band gap (3.2 eV for anatase) limits its utilization of sunlight and thus its practical applications in many important fields such as photocatalytic hydrogen evolution[5], environmental remediation[6] and solar energy conversion[7]. To overcome this barrier, great efforts have been devoted to engineer TiO_2's band gap from a variety of aspects in order to approach a high photoactivity under visible light irradiation. Introducing dopants is one of the most intensively investigated strategies to enhance its visible light utilization. Initially, metal ions were used as dopants to introduce states into the TiO_2 band gap[8–10], but the subsequential problems such as thermal instability, increased carrier recombination centers[11,12], and the need for an expensive ion-implantation facility significantly limit its applications. Nonmetal elements was also adopted[13,14], if doped under the right conditions, can effectively narrow band gap of TiO_2 and improve its visible-light absorption. Compared to other elements, nitrogen doping is thought to be the most useful choice to enhance its visible-light photocatalytic activity[15]. But unfortunately, further studies find that the activity of N-TiO_2 for visible-light induced hydrogen evolution is quite low[16].

Recently, the intrinsic defects in TiO_2 matrix such as oxygen vacancy (Vo) and Ti^{3+} have been proved to trigger the visible-light activity of TiO_2[17–24]. Chen *et al.*[17] have reported that hydrogen thermal treatment of TiO_2 nanoparticles can generate an amorphous layer near the surface to form defective black TiO_{2-x} nanoparticles. Such defective black TiO_{2-x} nanoparticles display excellent photoactivity and stability in photocatalytic hydrogen generation. Theoretical calculations demonstrate that high vacancy concentration could induce a vacancy band of electronic states just below the conduction band and

[1]Laboratory of Environmental Sciences and Technology, Xinjiang Technical Institute of Physics & Chemistry; Key Laboratory of Functional Materials and Devices for Special Environments, Chinese Academy of Sciences, Urumqi 830011, China. [2]University of Chinese Academy of Sciences, Beijing, 100049, China. Correspondence and requests for materials should be addressed to Y.Z. (email: zhuyq@ms.xjb.ac.cn) or C.W. (email: cywang@ms.xjb.ac.cn)

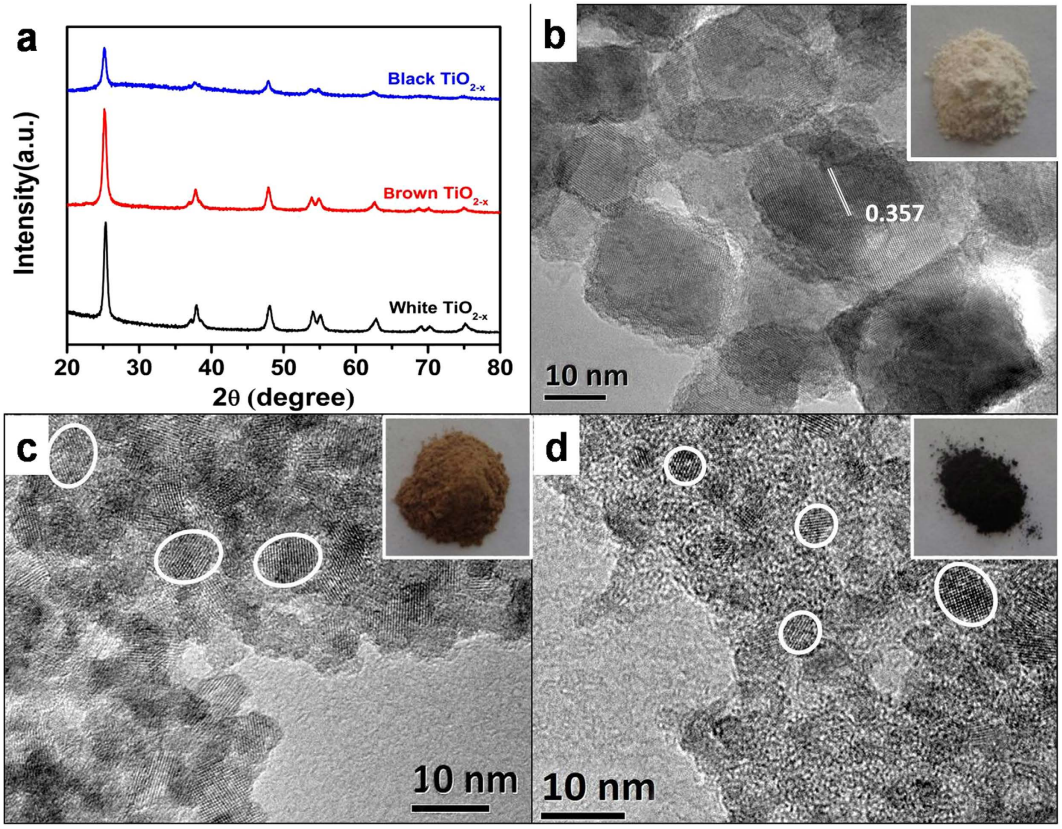

Figure 1. XRD patterns (a), TEM images (white TiO_{2-x}(b), brown TiO_{2-x}(c), black TiO_{2-x}(d)), of the defective TiO_{2-x} nanocrystals.

narrow the band gap to 1.0 eV. Except its optical and electronic properties, the performance of defective TiO_{2-x} also depends largely on its morphological and structural properties[25–27], like its surface area[28], particle size and pore structure[29]. However, to the best of our knowledge, rare work has been reported on controlling optical and morphological structure properties simultaneously for defective TiO_{2-x}. Herein, we report a facile hydrothermal approach to produce defective TiO_{2-x} nanocrystals with high surface area and tailoring band gap using $TiCl_3$ as a precursor and *L*-ascorbic acid as reductant and structure direction agent.

Results

The obtained defective TiO_{2-x} samples display diffraction peaks at 25.4°, 37.9°, 48.1° and 53.1° in the XRD patterns, indicating that as synthesized TiO_{2-x} is in a pure anatase phase (Fig. 1a). It suggests that the presence of *L*-ascorbic acid does not influence the crystal structure of TiO_{2-x}. TEM analysis with the obtained defective TiO_{2-x} samples shows that the particle size of highly crystallized TiO_2 core gradually decreases from 50 nm to 10 nm (Figs. 1b-1d) as increasing the amount of *L*-ascorbic acid from 0, 0.3 to 0.7 g in 80 mL solution. The crystal lattices of TiO_2 core can be clearly identified in all the samples, indicating that the TiO_2 core is highly crystallized. Since the particles are overlapped, the disordered TiO_{2-x} outer layer cannot be distinguished in TEM, but its presence can be indirectly confirmed via further sintering of the defective black TiO_{2-x} at 500 °C in N_2 atmosphere considering that high concentration of vacancy could significantly reduce the melting temperature of TiO_2[25,26]. The sintered TiO_{2-x} exhibits a nanoscroll structure with several layers of TiO_{2-x} sheets and the interlayer spacing is 0.76 nm (see Fig. S1a for details). EDX measurement (Fig. S1b) confirms that the TiO_{2-x} nanoscroll is only composed of Ti (56.4 at%) and O (28.8 at%) elements, implying the presence of defective TiO_{2-x} layer surrounding the TiO_2 core. It is worth to mention, the defective TiO_{2-x} nanosheet is a fascinating structure to apply in Li-ion battery and photocatalysis for its ultrahigh cycle rate and high efficiency[30,31]. This report provides a new and simple method for preparing the defective TiO_{2-x} nanosheets.

The N_2 adsorption–desorption isotherms (Fig. 2a) of defective TiO_{2-x} samples exhibit a typical type-IV isotherm with a distinct hysteretic loop, indicating mesoporous features. The average pore size (Fig. 2b) decreases with increasing the amount of added *L*-ascorbic acid, while the corresponding BET surface area (Tab. S1) dramatically increases from 64.56 $m^2\ g^{-1}$ (white TiO_{2-x}), 188.75 $m^2\ g^{-1}$ (brown TiO_{2-x}) to 263.95 $m^2\ g^{-1}$ (black TiO_{2-x}). Therefore, the presence of *L*-ascorbic acid molecules significantly affects the

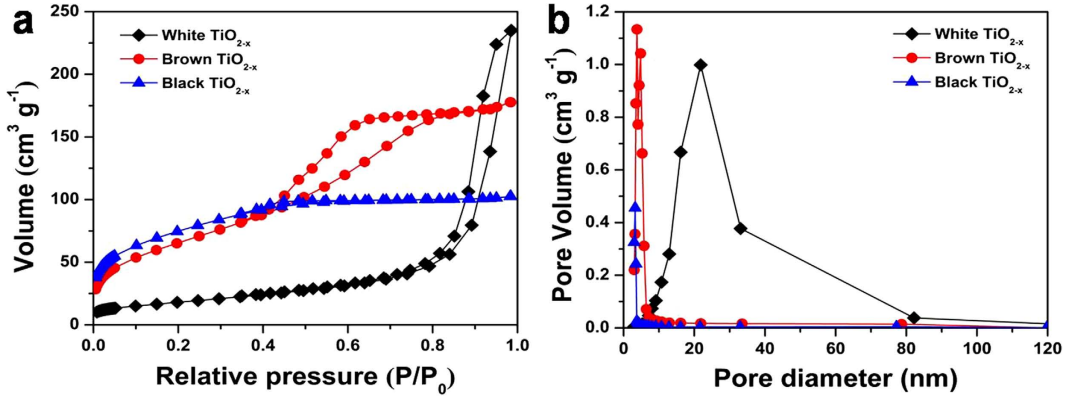

Figure 2. N_2 adsorption–desorption isotherms (a) and pore size distribution (b) of the defective TiO_{2-x} nanocrystals.

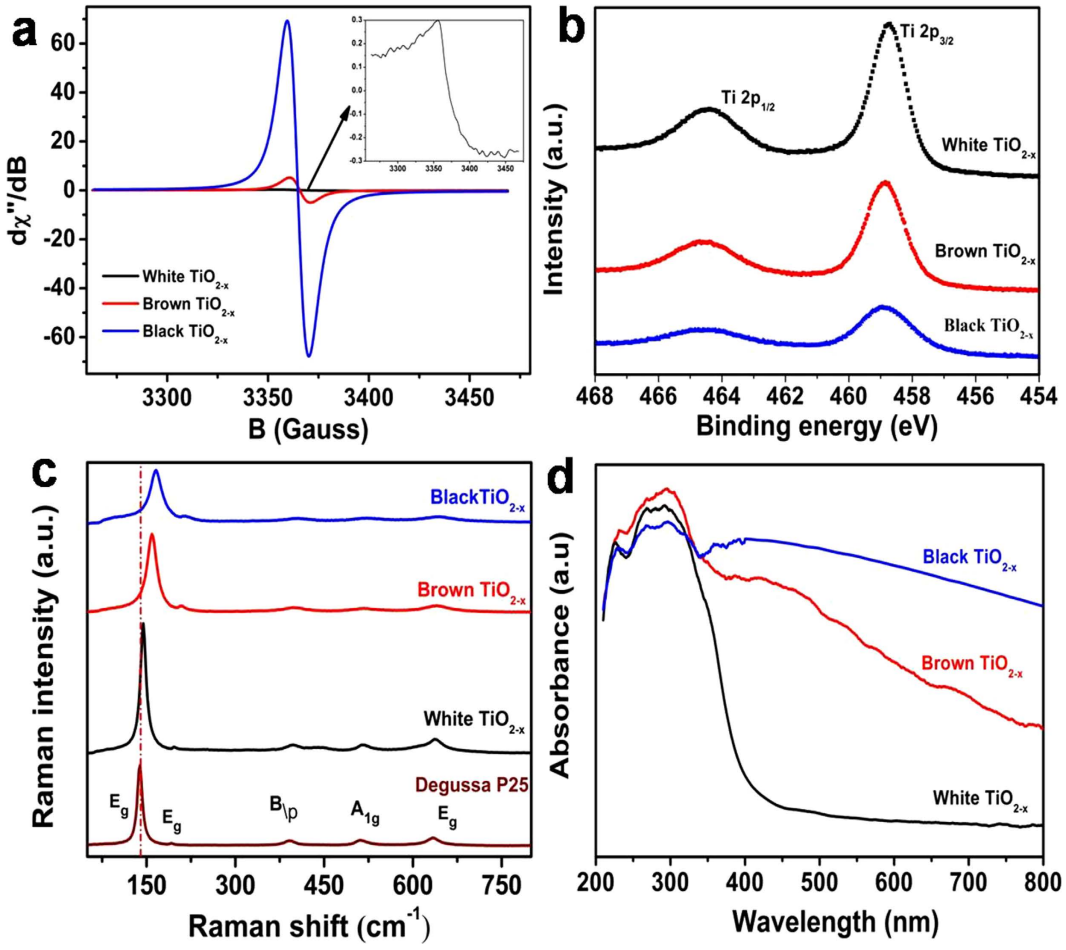

Figure 3. EPR (a), XPS (b), Raman (c), and DRS (d) profiles of the defective TiO_{2-x} nanocrystals.

pore structure and surface area of the obtained TiO_{2-x} samples. The porous structure makes the defective TiO_{2-x} materials suitable for photocatalysis application because of their abundant porous channels.

Electron paramagnetic resonance (EPR) measurements were conducted at room temperature to verify the presence of high concentration Vo. As shown in Fig. 3a, all the defective TiO_{2-x} samples show a very strong EPR signal at *g*-value of 2.003 which indicates the significant presence of Vo. As discussed previously, the EPR signal appearing at *g*-value of 2.003 is caused by electrons trapped on surface Vo[32,33]. However, the representative signal of Ti^{3+} usually appearing at $g \approx 1.94$[34,35] is not shown here, which suggests the absence of rhombic Ti^{3+} in defective TiO_{2-x} samples. Furthermore, the EPR signals of brown

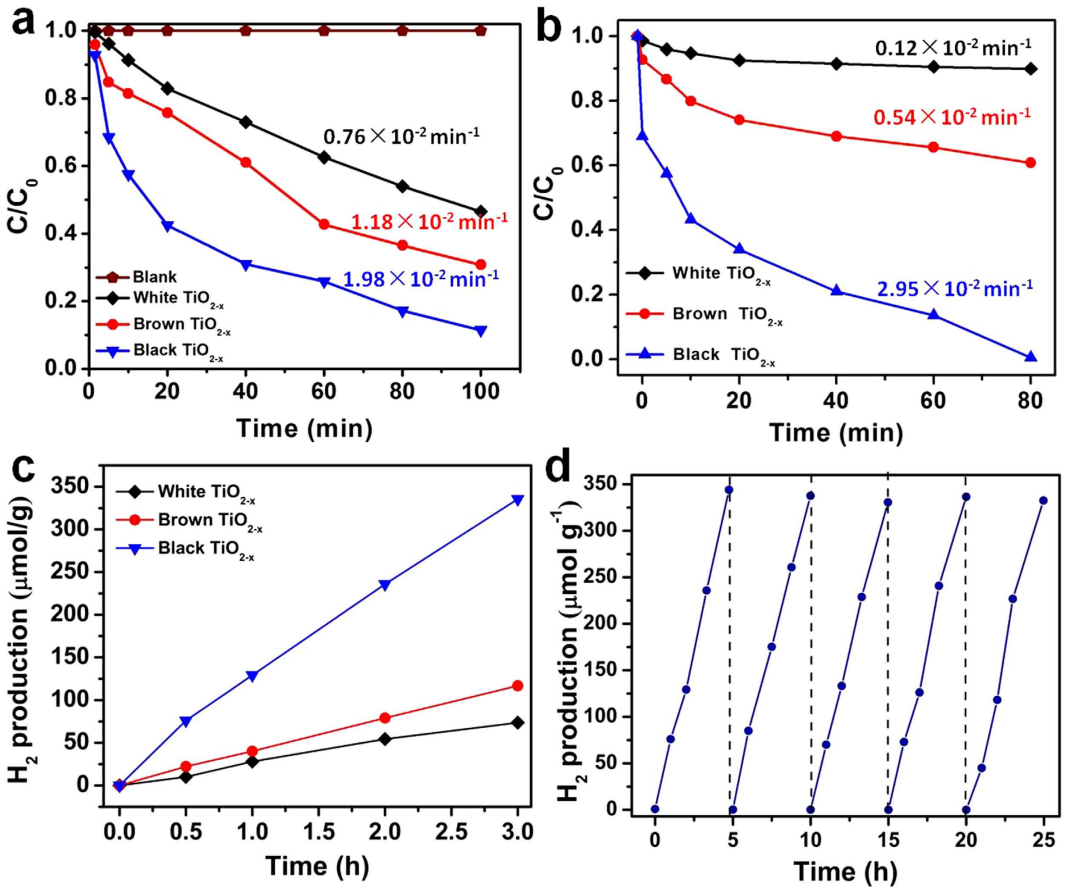

Figure 4. Degradation of MB (a) and phenol (b), hydrogen evolution (c) and cycle test (d) of the defective TiO_{2-x} nanocrystals under visible light (>420 nm) .

and black TiO_{2-x} show a great enhancement in the intensity, which indicates their substantially increased Vo concentrations due to the increase in the amount of added *L*-ascorbic acid. Therefore, the defects in the colorful TiO_{2-x} are present as Vo instead of Ti^{3+}. X-ray photoelectron spectroscopy (XPS) characterization of the white, brown and black TiO_{2-x} samples (Fig. 3b) shows only $Ti2p_{1/2}$ and $Ti2p_{3/2}$ peaks with slightly difference but no Ti^{3+} peaks appeared, which further confirms that Ti^{3+} does not exist in the defective TiO_{2-x} nanocrystals. Structural properties of the obtained TiO_{2-x} samples were further examined by measuring Raman scattering. For comparison, P25 Degussa was also analyzed. As shown in Fig. 3c, the six (3Eg + 2B1g + A1g) Raman-active modes of anatase phase with frequencies at 144, 197, 399, 515, 519 (superimposed with the 515 cm^{-1} band), and 639 cm^{-1} were detected in all investigated samples. Compared with P25, the defective TiO_{2-x} nanocrystals display a varying degree of blue-shift in Raman bands (Eg from 139 to 144, 153 and 164 cm^{-1}, respectively), which indicates that the original symmetry of TiO_2 lattice is broken down due to the disordered TiO_{2-x} layer formed by introducing of *L*-ascorbic acid[36]. In addition, the peak shift of defective TiO_{2-x} gradually increases along with the darkening color, suggesting the increase in the Vo concentration. This result further supports that the Vo concentration could be controlled by the amount of *L*-ascorbic acid directly. The optical property of all the defective TiO_{2-x}powder samples was characterized by UV-visible diffuse reflectance spectra (DRS), as shown in Fig. 3d. The white TiO_{2-x}exhibits a strong absorption in the UV range, while the brown and black TiO_{2-x} samples display a broad absorption over the entire UV-vis wavelength range investigated. Furthermore, the black TiO_{2-x} sample shows even higher absorption of UV-vis light than the brown TiO_{2-x} sample which further confirms the assumption that the high concentration of Vo is capable of generating a new vacancy band locating just below the conduction band edge of pure TiO_2.

The photocatalytic degradation of MB (20 mg/L) and phenol (10 mg/L) was performed using 0.5 g/L of the as-synthesized white, brown and black TiO_{2-x} powders under a 300 W Xenon lamp with UV cut-off filter ($\lambda > 420$ nm). As shown in Figs. 4a and 4b, the black TiO_{2-x} exhibits the highest efficiency in both MB and phenol degradation. The kinetic reaction rate of MB degradation at black TiO_{2-x} is 1.98×10^{-2} min^{-1}, while it is 1.18×10^{-2} min^{-1} at the brown TiO_{2-x}, and 0.76×10^{-2} min^{-1} at the white TiO_{2-x}. Similar improvement was also observed for phenol degradation, the kinetic rate at black $TiO_{2-x}$is 2.95×10^{-2} min^{-1}, which is about 25.41 times greater than that at white TiO_{2-x}. The phenol molecules could be totally decomposed at black TiO_{2-x} nanocrystals under visible light irradiation in about 80 min.

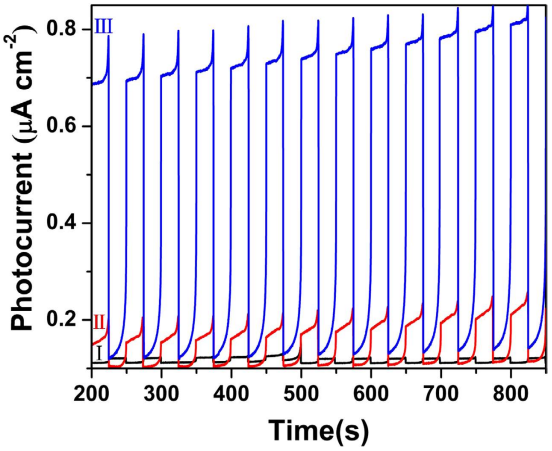

Figure 5. Photocurrent (I: white TiO_{2-x}; II: brown TiO_{2-x}; III: black TiO_{2-x}) of the defective TiO_{2-x} nanocrystals under visible light (>420 nm).

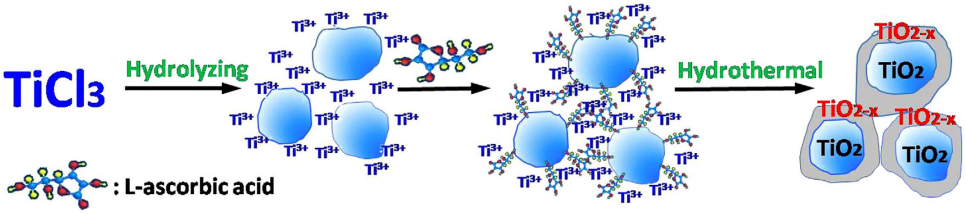

Figure 6. Schematic diagram for the formation of defective TiO_{2-x} nanocrystals.

Moreover, the photocatalytic activity of the defective TiO_{2-x} was also tested for hydrogen generation under visible light (Fig. 4c). All the catalysts were loaded with 0.6 wt% Pt, and methanol was used as sacrificial agent. The black TiO_{2-x} nanocrystals show a much higher photocatalytic activity with a hydrogen evolution rate of 116.7 μmol g^{-1} h^{-1} compared to the white TiO_2 (20.6 μmol g^{-1} h^{-1}) and brown TiO_{2-x} (38.9 μmol g^{-1} h^{-1}) under visible light irradiation in the presence of 20 mg/L photocatalyst. The cycling test results of the visible-light driven photocatalytic activity of black TiO_{2-x} nanocrystals for hydrogen evolution as a function of time during a 25-hour testing period are shown in Fig. 4d. No noticeable decrease in H_2 production rate for black TiO_{2-x} in 5 cycle tests were observed within the test period, indicating good stability of the black TiO_{2-x} nanocrystals in the photocatalytic production of hydrogen from water under visible light. The photocatalysis results confirm that the presence of defective TiO_{2-x} outer layer with well-developed porosity is the key factor leading to improved photoactivity. The high Vo concentration in the defective TiO_{2-x} nanocrystals enhances the absorption of visible light and thereby the generation of charge carriers, which are further transformed into abundant active species of $\cdot O_2^-$ and ·OH to degrade the pollutants and split water to produce H_2 under the visible light irradiation. The high surface area and rich pore structure increase the collision possibility of the pollutant molecules with catalyst surface and the adsorbed active radicals. These factors are responsible for the enhancement of photocatalytic activity of defective TiO_{2-x} nanocrystals for pollutants degradation and hydrogen evolution. This is further confirmed by the measurement of photocurrent densities with the defective TiO_{2-x} nanocrystals photoanodes at a constant potential of 0 V (vs Ag/AgCl) under visible light (Figs. 5 and 6). The photocurrent density of black TiO_{2-x} is the highest in all the samples, which is almost 10 times of that of white TiO_{2-x}. Thus, the high concentration of Vo defects gives rise to high visible-light induced photo-electron transformation and results in high efficiency in photocatalytic activity.

Discussion

Due to its unique optical property and superior visible-light-driven photocatalytic activity, defective TiO_{2-x}, has attracted plenty of attentions recently. But most of the reports focused on tailoring the photochemical properties, rare study is reported on its structure and morphology. To the best of our knowledge, the highest surface area of defective TiO_{2-x} reported was near 90 m^2/g[37]. In this report, we presented a novel method for fabricating defective TiO_{2-x} nanocrystals with tunable bandgap and high surface area using Ti(III)-salt as a precursor and *L*-ascorbic acid as reductant and structure direction agent. The formation of defective TiO_{2-x} nanocrystals is schematically shown in Fig. 5. During hydrolysis, the -$TiOH^{2+}$ was formed first (Eq. 1) and oxidized by the dissolved oxygen to the Ti(IV)-oxo species (Eq. 2)[38], and *L*-ascorbic acid molecules were adsorbed on the initial particle surface through

Ti-O-C bond, while the excessive Ti^{3+} was diffused in the interspace of *L*-ascorbic acid molecules. The Ti(IV)-oxo species is assumed to be an intermediate between TiO^{2+} and TiO_2, consisting of partially dehydrated polymeric Ti(IV)hydroxide[39]. Following hydrothermal process, Ti(IV)-oxo was transferred to highly crystallized TiO_2 (Eq. 3). If without the presence of *L*-ascorbic acid molecules, the excessive Ti^{3+} would react with the dissolved oxygen molecules in the solution to grow into TiO_2 crystals. But the chemical adsorption of *L*-ascorbic acid inhibited the diffusion of dissolved oxygen molecules to the TiO_2 core surface, and hindered the growth of TiO_2 crystals[40,41]. Since the oxidation process suffered from the insufficient supply of oxygen, after removing the adsorbed *L*-ascorbic acid, Vo was produced outside of the TiO_2 core[20]. Therefore, a defective, nonstoichiometric TiO_{2-x} layer was formed surround the TiO_2 core with rich oxygen vacancies. In addition, abundant pore structures were formed in the defective TiO_{2-x} layer after removing the adsorbed *L*-ascorbic acid, evidencing its critic role as a structure direction agent.

$$Ti^{3+} + H_2O \rightarrow TiOH^{2+} + H^+ \quad (1)$$

$$TiOH^{2+} + O_2 \rightarrow \text{Ti(IV) oxo species} + O_2^- \quad (2)$$

$$\text{Ti(IV) oxo species} \xrightarrow{\text{hydrothermal}} TiO_2 \quad (3)$$

In summary, a facile hydrothermal approach has been developed for preparing defective TiO_{2-x} nanocrystals with $TiCl_3$ as a precursor. *L*-ascorbic acid plays critical role in controlling the morphology and bandgap structure towards engineering the prepared defective TiO_2. The defects in the defective TiO_{2-x} nanocrystals proved to be of Vo, while the Vo concentration and band gap of the defective TiO_{2-x} nanocrystals could be easily tailored by varying the introduced amount of *L*-ascorbic acid. Comparing with the white and brown defective TiO_{2-x}, the black TiO_{2-x} shows much higher surface area and efficiency in degradation of organic pollutants (MB and phenol) and hydrogen evolution under visible light irradiation. The present work provides an alternative approach for fabricating defective TiO_{2-x} nanocrystal photocatalysts with controllable band gap and morphological structure for environmental remediation and solar fuel generation.

Method

Materials synthesis. For the preparation of reduced TiO_2 nanocrystals, different amounts of L-ascorbic acid (0, 0.3 g and 0.7 g) were added to 70 mL DI water and stirred for 10 min at RT. Subsequently, 3.1 mL of $TiCl_3$ was added and a purple solution was formed. Then, NaOH solution (1 mol/L) was added to raise the pH to 4. After stirring for another 30 min at RT, the mixture was transferred to a 100 mL Teflon-lined stainless steel autoclave and heated at 180 °C for 12 h. The obtained precipitates were collected by centrifugation, rinsed with water and ethanol for several times. After drying at 80 °C for overnight, the defective TiO_{2-x} samples were labeled according to its color as white, brown and black TiO_{2-x}.

Characterization. X-ray diffraction (XRD) patterns of the samples were collected on Bruker D8 Advance powder diffractometer over scattering angles from 20° to 80° using Cu Kα radiation. Transmission electron microscopy (TEM) characterization was performed on a JEOL-JEM 2100 electron microscope. Optical property was examined by UV−Visible diffuse reflectance spectrophotometer (DRS) (Shimadzu SolidSpec-3700DUV). The electron paramagnetic resonance (EPR) spectra were characterized with Bruker E500 Spectrophotometer. X-ray photoelectron spectra (XPS) of the samples were measured using a Kratos Analytical AMICUS XPS instrument.

Methylene blue (MB) and phenol degradation. 40 mL MB (20 mg/L) solution or phenol solution (10 mg/L) was placed in a 50 mL quartz photoreactor. The photocatalyst (0.5 g/L) was dispersed into the solution at neutral pH. In order to attain adsorption-desorption equilibrium, the solution was stirred in dark for 40 min. The solution was then irradiated by a 300 W Xenon lamp with UV cut-off filter ($\lambda > 420$ nm) at RT. Samples were taken at given time interval to test the concentration of MB and phenol. The concentration of MB was measured by UV-visible spectrophotometer (UV-1800, Shimadzu). The phenol concentration was determined by Thermo Fisher Ultra 3000 HPLC equipped with a 25 cm × 4.6 mm Cosmosil C18 column.

Photocatalytic hydrogen evolution. The photocatalytic reactions of H_2 evolution were carried out in a closed gas circulation system with an external-irradiation type of a glass reactor. The light source was a 300 W Xenon lamp with UV cut-off filter ($\lambda > 420$ nm). The co-catalyst Pt was loaded by an in-situ photodeposition method. The 0.6 wt% of Pt-loaded catalyst (25 mg) was dispersed with a magnetic stirrer in a methanol aqueous solution (10 mL of CH_3OH and 90 mL of H_2O). The evolved gas including H_2 was analyzed using an online gas chromatograph (7890A, Agilent) equipped with a thermal conductivity detector (TCD).

Photocurrent measurement. The photocurrent was performed with an electrochemical instrument CHI660E using a three-electrode system. The samples (0.1 g) were loaded on conductive surface of ITO glass and 0.5 M Na_2SO_4 solution was used as electrolyte. 300 W Xenon lamp equipped with UV cut-off filter ($\lambda > 420$ nm) was used as light source, and standard calomel electrode (SCE) as reference electrode, Pt slice as counter electrode.

References

1. Fujishima, A. & Honda, K. Electrochemical Photolysis of Water at a SemiconductorElectrode. *Nature* **238,** 37–38 (1972).
2. Chen, X. & Mao, S. S. Titanium dioxide nanomaterials: synthesis, properties,modifications, and applications. *Chem. Rev.* **107,** 2891–2959 (2007).
3. Hoffmann, M. R., Martin, S. T. & Bahnemannt, D. W. Environmental Applications of Semiconductor Photocatalysis. *Chem. Rev.* **95,** 69–96 (1995).
4. Yang, D. *et al.* An Efficient Photocatalyst Structure: TiO_2(B) Nanofibers with a Shell of Anatase Nanocrystals. *J. Am. Chem. Soc.* **131,** 17885–17893 (2009).
5. Manivannan, A. & Wu, N. Solar Hydrogen Generation by a CdS-Au-TiO_2 Sandwich Nanorod Array Enhanced with Au Nanoparticle as Electron Relay and Plasmonic Photosensitizer. *J. Am. Chem. Soc.* **136,** 8438–8449 (2014).
6. Alvaro, M., Aprile, C., Benitez, M., Carbonell, E. & García, H. Photocatalytic Activity of Structured Mesoporous TiO_2 Materials. *J.Phys. Chem. B* **110,** 6661–6665 (2006).
7. Zhang, J., Bang, J., Tang, C. & Kamat, P. V. Tailored TiO_2-$SrTiO_3$ Heterostructure Nanotube Arrays for Improved Photoelectrochemical Performance. *ACS Nano* **4,** 387–395 (2010).
8. Li, J. *et al.* Synthesis, Characterization, and Visible Light Activity of New Nanoparticle Photocatalysts Based on Silver, Carbon, and Sulfur-doped TiO_2. *J. Colloid Interface Sci.* **311,** 514–522 (2007).
9. Valero, J. M., Obregón, S. & Colón, G. Active Site Considerations on the Photocatalytic H_2 Evolution Performance of Cu-Doped TiO_2 Obtained by Different Doping Methods. *ACS Catal.* **4,** 3320–3329 (2014).
10. Hamedani, H. A., Allam, N. K., Garmestani, H. & El-Sayed, M. A. Electrochemical Fabrication of Strontium-Doped TiO_2 Nanotube Array Electrodes and Investigation of Their Photoelectrochemical Properties. *J. Phys. Chem. C* **115,** 13480–13486 (2011).
11. Zheng, Z. *et al.* Facile *in situ* Synthesis of Visible-light Plasmonic Photocatalysts M@TiO_2 (M=Au, Pt, Ag) and Evaluation of Their Photocatalytic Oxidation of Benzene to Phenol. *J. Mater. Chem.* **21,** 9079–9087 (2011).
12. Xu, P. *et al.* I_2-Hydrosol-Seeded Growth of $(I_2)_n$-C-Codoped Meso/Nanoporous TiO_2 for Visible Light-Driven Photocatalysis. *J. Phys. Chem. C* **114,** 9510–9517 (2010).
13. Toro, C. & Buriak, J. M. F^- Doping on TiO_2 Provided Important Insights into Photocatalysis. *Chem. Mater.* **27,** 1443–1444 (2015).
14. Wang, F., Jiang, Y., Gautam, A., Li, Y. & Amal, R. Exploring the Origin of Enhanced Activity and Reaction Pathway for Photocatalytic H_2 Production on Au/B-TiO_2 Catalysts. *ACS Catal.* **4,** 1451–1457 (2014).
15. Asahi, R., Morikawa, T., Ohwaki, T., Aoki, K. & Taga, Y. Visible-light photocatalysis in nitrogen-doped titanium oxides. *Science* **293,** 269–271 (2001).
16. Gopal, N. O., Lo, H. H. & Ke, S. C. Chemical State and Environment of Boron Dopant in B,N-Codoped Anatase TiO_2 Nanoparticles: An Avenue for Probing Diamagnetic Dopants in TiO_2 by Electron Paramagnetic Resonance Spectroscopy. *J. Am. Chem. Soc.* **130,** 2760–2761 (2008).
17. Chen, X., Liu, L., Yu, Y. P. & Mao, S. S. Increasing Solar Absorption for Photocatalysis with Black Hydrogenated Titanium Dioxide Nanocrystals. *Science* **331,** 746–750 (2011).
18. Zuo, F. *et al.* Self-Doped Ti^{3+} Enhanced Photocatalyst for Hydrogen Production under Visible Light. *J. Am. Chem. Soc.* **132,** 11856–11857 (2010).
19. Wendt, S. *et al.* The Role of Interstitial Sites in the Ti3d Defect State in the Band Gap of Titania. *Science* **320,** 1755–1759 (2008).
20. Chen, C. C., Say, W. C., Hsieh, S. J. & Diau, E. W. A Mechanism for the Formation of Annealed Compact Oxide Layers at the Interface Between Anodic Titania Nanotube Arrays and Ti Foil. *Appl. Phys.* **A95,** 889–898 (2009).
21. Su, J. *et al.* Porous Titania with Heavily Self-Doped Ti^{3+} for Specific Sensing of CO at Room Temperature. *Inorg. Chem.* **52,** 5924–5930 (2013).
22. Xia, T., Zhang, Y., Murowchick, J. & Chen, X. Vacuum-treated titanium dioxide nanocrystals: Optical properties, surface disorder, oxygen vacancy, and photocatalytic activities. *Catal. Today* **225,** 2–9 (2014).
23. Liu, L. & Chen, X. Titanium Dioxide Nanomaterials: Self-Structural Modifications. *Chem. Rev.* **114,** 9890–9918 (2014).
24. Chen, X., Liu, L. & Huang, F. Black titanium dioxide (TiO_2) nanomaterials. *Chem. Soc. Rev.* **44,** 1861–1885 (2015).
25. Srivastava, S. *et al.* Size-Selected TiO_2 Nanocluster Catalysts for Efficient Photoelectrochemical Water Splitting. *ACS Nano* **8,** 11891–11898 (2014).
26. Lang, S. M. & Bernhardt, T. M. Gas Phase Metal Cluster Model Systems for Heterogeneous Catalysis. *Phys. Chem. Chem.Phys.* **14,** 9255–9269 (2012).
27. Jun, Y. W. *et al.* Surfactant-assisted elimination of a high energy facet as a means of controlling the shapes of TiO_2 nanocrystals. *J. Am. Chem. Soc.* **125,15981**–15985 (2003).
28. Qiu, B. *et al.* Facile Synthesis of the Ti^{3+} Self-doped TiO_2-graphene Nanosheet Composites with Enhanced Photocatalysis. *Sci. Rep.* **5,** 8591–8596 (2015).
29. Su, J. *et al.* Porous Titania with Heavily Self-Doped Ti^{3+} for Specific Sensing of CO at Room Temperature. *Inorg. Chem.* **52,** 5924–5930 (2013).
30. Myung, S. T. *et al.* Black Anatase Titania Enabling Ultra High Cycling Rates for Rechargeable Lithium Batteries. *Energy Environ. Sci.* **6,** 2609–2614 (2013).
31. Chen, J. S. *et al.* Constructing Hierarchical Spheres from Large Ultrathin Anatase TiO_2Nanosheets with Nearly 100% Exposed (001) Facets for Fast Reversible Lithium Storage. *J. Am. Chem. Soc.* **132,** 6124–6130 (2010).
32. Randorn, C. & Irvine, J. T. S. Synthesis and Visible Light Photoactivity of a High Temperature Stable Yellow TiO_2 Photocatalyst. *J. Mater. Chem.* **20,** 8700–8704 (2010).
33. Naldoni, A. *et al.* Pt and Au/TiO_2 Photocatalysts for Methanol Reforming: Role of Metal Nanoparticles in Tuning Charge Trapping Properties and Photoefficiency. *Appl. Catal. B* **130,** 239–248 (2013).
34. Hoang, S., Berglund, S. P., Hahn, N. T., Bard, A. J. & Mullins, C. B. Enhancing Visible Light Photo-oxidation of Water with TiO_2 Nanowire Arrays via Cotreatment with H_2 and NH_3: Synergistic Effects between Ti^{3+} and N. *J. Am. Chem. Soc.* **134,** 3659–3662 (2012).
35. Grabstanowicz, L. R. *et al.* Facile Oxidative Conversion of TiH_2 to High-Concentration Ti^{3+}-Self-Doped Rutile TiO_2 with Visible-Light Photoactivity. *Inorg. Chem.* **52,** 3884–3890 (2013).
36. Dong, J. *et al.* Defective Black TiO_2 Synthesized via Anodization for Visible-Light Photocatalysis. *ACS Appl. Mater. Interfaces* **6,** 1385–1388 (2014).

37. Ren, R. *et al.* Controllable Synthesis and Tunable Photocatalytic Properties of Ti^{3+}-doped TiO_2. *Sci. Rep.* **5,** 10714–10724 (2015).
38. Hosono, E., Fujihara, S., Kakiuchi, K. & Imai, H. Growth of Submicrometer-Scale Rectangular Parallelepiped Rutile TiO_2 Films in Aqueous $TiCl_3$ Solutions under Hydrothermal Conditions. *J. Am. Chem. Soc.* **126,** 7790–7791 (2004).
39. Kavan, L., O'Regan, B., Kay, A. & Gratzel, M. Preparation of TiO_2 (anatase) Films on Electrodes by Anodic Oxidative Hydrolysis of $TiCl_3$. *J. Electroanal. Chem.* **346,** 291–307 (1993).
40. Prakasam, H. E., Shankar, K., Paulose, M., Varghese, O. K. & Grimes, C. A. A New Benchmark for TiO_2 Nanotube Array Growth by Anodization. *J. Phys. Chem.C* **111,** 7235–7241 (2007).
41. Paulose, M. *et al.* Anodic Growth of Highly Ordered TiO_2 Nanotube Arrays to 134μm in Length. *J. Phys. Chem. B* **110,** 16179–16184 (2006).

Acknowledgements

This work was supported by the National Nature Science Foundation of China (Grant No. 21173261), the "Western Light" Program of Chinese Academy of Sciences (XBBS201410), the CAS/SAFEA International Partnership Program for Creative Research Teams, the CAS "Western Action Plan" (KGZD-EW-502), and the High-Technology Research & Development Project of Xinjiang Uyghur Autonomous Region (201415110).

Author Contributions

M.W.S. and Y.Z. performed the experiments and wrote the main manuscript text. C.W. guided the whole work. X.F., J.Z., Y.L. made contribution for discussions and critical revision of the manuscript. J.Z. also tested the BET measurement, and S.A. assisted the photocurrent measurements. All authors reviewed the manuscript.

Additional Information

Supplementary information accompanies this paper at http://www.nature.com/srep

Competing financial interests: The authors declare no competing financial interests.

How to cite this article: Wajid Shah, M. *et al.* Facile Synthesis of Defective TiO_{2-x} Nanocrystals with High Surface Area and Tailoring Bandgap for Visible-light Photocatalysis. *Sci. Rep.* **5**, 15804; doi: 10.1038/srep15804 (2015).